frontiers in Nanotechnology

ORIGINAL RESEARCH
published: 20 November 2020
doi: 10.3389/fnano.2020.592739

A Streamlined Study on Chitosan-Zinc Oxide Nanomicelle Properties to Mitigate a Drug-Resistant Biofilm Protection Mechanism

Alya Limayem[1,2]*, *Shrushti B. Patil*[1], *Mausam Mehta*[1,3], *Feng Cheng*[1] and *Minh Nguyen*[1,2]

[1] Department of Pharmaceutical Sciences, College of Pharmacy, University of South Florida, Tampa, FL, United States, [2] Division of Translational Medicine, Center for Education in Nanobioengineering, University of South Florida, Tampa, FL, United States, [3] MD Program, Morsani College of Medicine, University of South Florida, Tampa, FL, United States

The nosocomial multidrug resistant bacteria (MDR), are rapidly circulating from water surfaces to humans away from the clinical setting, forming a cyclical breeding ground of resistance, causing worldwide infections, and thus requiring urgent responses. The combination of chitosan and zinc oxide (CZNPs), with proven bactericidal effects on some MDRs, was further studied to set the stage for a broad-spectrum *in vivo* utilization of CZNPs. Toward ensuring CZNPs' uniformity and potency, when it faces not only biofilms but also their extracellular polymeric substances (EPS) defense mechanism, the size, zeta potential, and polydispersity index (PDI) were determined through dynamic light scattering (DLS). Furthermore, the efficacy of CZNPs was tested on the inhibition of MDR Gram-negative *Escherichia coli* BAA-2471 and Gram-positive *Enterococcus faecium* 1449 models, co-cultured in an Alvatex 3D fiber platform as a biofilm-like structure. The Biotek Synergy Neo2 fluorescent microplate reader was used to detect biofilm shrinkage. The biofilm protection mechanism was elucidated through detection of EPS using 3D confocal and transmission electronic microscopy. Results indicated that 200 μl/mL of CZNPs, made with 50 nm ZnO and 10,000 Da chitosan ($N = 369.1$ nm; PDI = 0.371; zeta potential = 22.8 mV), was the most promising nanocomposite for MDR biofilm reduction, when compared to CZNPs enclosing ZnO, 18 or 100 nm. This study depicts that CZNPs possess enough potency and versatility to face biofilms' defense mechanism *in vivo*.

Keywords: multi-drug resistance, nanotherapeutics, chitosan, zinc oxide, dynamic light scattering, TEM microscopy, 3D confocal microscopy, physico-chemical properties

OPEN ACCESS

Edited by:
Raghvendra Ashok Bohara, National University of Ireland Galway, Ireland

Reviewed by:
Won Min Park, Kansas State University, United States
Vijayakumar Sekar, Shandong University, Weihai, China

***Correspondence:**
Alya Limayem
alimayem@usf.edu

Specialty section:
This article was submitted to Biomedical Nanotechnology, a section of the journal Frontiers in Nanotechnology

Received: *07 August 2020*
Accepted: *23 October 2020*
Published: *20 November 2020*

Citation:
Limayem A, Patil SB, Mehta M, Cheng F and Nguyen M (2020) A Streamlined Study on Chitosan-Zinc Oxide Nanomicelle Properties to Mitigate a Drug-Resistant Biofilm Protection Mechanism. Front. Nanotechnol. 2:592739. doi: 10.3389/fnano.2020.592739

INTRODUCTION

During recent decades, interest in nanotherapeutics in the United States and worldwide has met an unprecedented progress in biomedical and food safety fields (Ponce et al., 2018). Of particular evolution are emerging nanotherapeutics for infectious diseases, of which the nosocomial multidrug resistant bacteria constitute a serious threat to public health as they are proliferating exponentially from clinical settings to wastewaters and their surrounding environment.

Among the MDR pathogens, some strains of multidrug resistant fecal bacteria (MRFs), including both Gram-positive *Enterococcus faecium* and Gram-negative *Escherichia coli*, are the main causatives of hospital-acquired infections. Recent concerns arose from MRF biofilm formation within indwelling-catheter devices in hospitals, which was primarily associated with urinary tract infection (Sabir et al., 2017). According to the CDC, from data in 2017, Clonal Complex 17 (CC17) Vancomycin-resistant *E. faecium* (VRE) strain alone has caused more than 54,500 hospitalizations and 5,400 deaths per annum (CDC, 2019). Aside from clinical settings, it was also found abundantly in some reclaimed wastewaters and food animals (Tree et al., 2003; Yu and Zhang, 2012; Fahrenfeld et al., 2013; Pruden et al., 2013; Limayem, 2015; Limayem et al., 2015a). Among its many virulence factors, the biofilm-forming capabilities of MDR CC17 beyond Vancomycin-Resistant Enterococci (VRE) are particularly concerning, and thought to be related to the presence of Endocarditis- and biofilm-associated bacterial pili, which allow for bacterial adhesion to facilitate biofilm formation (Arias and Murray, 2012). The considerable phenotypical elasticity and antigenic variance of this "Superbug" generate out from it an enormous "factory" of continuous antibiotic resistance production. Owing to these increasing public health risks, it is deemed imperative to develop an alternative antimicrobial over conventional antibiotics that is broad-spectrum and cost-efficient in order to suppress both Gram-positive and Gram-negative MDR strains with minimal side effects and a high safe threshold toxicity. Among the most promising nanotherapeutics, the newly designed CZNPs have been proven to have an extraordinary inhibitive potential against a substantial number of pathogens and MDR strains primarily nosocomial multidrug resistant *Enterococcus faecium*, *Esherchia coli,* and *Pseudomonas* spp. (Limayem et al., 2015a,b; Mehta et al., 2019; Mohapatra and Limayem, 2019).

The field of nanotechnology has evolved over the last decade, especially with the discoverance of metal nanoparticle utility in various applications, including those that are diagnostic, such as their role in the enhancement of microarray systems, fluorescent agents and magnetic resonance imaging contrast agents (Dixit et al., 2012; Roy et al., 2012; Ni et al., 2017), as well as those that are therapeutic. This study in particular places an emphasis on ZnO nanoparticles and their synergistic therapeutic effects with chitosan on MDR biofilms. Although the effectiveness of chitosan or ZnO alone against some pathogens has been extensively documented (Premanathan et al., 2011; AbdElhady, 2012; Al-Naamani et al., 2017), and some studies have demonstrated the effectiveness of non-nanomicellar chitosan-zinc oxide composites (Khan et al., 2008; AbdElhady, 2012; Dhillon et al., 2014; Rahman et al., 2015), little is known about their physico-chemical properties pertaining to their uniformity, stability and monodispersity, which are crucial to ensure efficacy when CZNPs is tested against bacterial biofilm correlated to the extracellular polymeric substances (EPS) defense mechanism. While chitosan is a biodegradable polymer with demonstrated antiseptic properties against Gram-negative strains including *E. coli* as well as other properties such as mucoadhesiveness, bioadhesiveness, antimicrobial properties, and cationic interactions with metal oxides, which make it an ideal nanodrug pertaining to drug delivery and against various cancers (Knorr, 1983; Limayem et al., 2011; Vashist et al., 2013; Zhang et al., 2016; Gupta et al., 2017; Sharma et al., 2018), ZnO is an emerging nanocomponent that is known for its effectiveness with some cancer cells as well as its selective antimicrobial properties toward Gram-positive bacteria (Premanathan et al., 2011). The nanomicellar joint CZNPs' uniqueness arise from their synergistic effects against a broad spectrum of MDR pathogens and flexibility to cope with different host cells depending on their structure, concentration, molecular weight, and size (Mohapatra and Limayem, 2019). As far as CZNPs go for the treatment of the gastrointestinal tract (GIT)-located MRFs, a nanomicellar structure was evidenced to be effective *in vitro* against biofilms formed in a 3D scaffold, mimicking the *in vivo* structure of the collagen matrix found in the GIT (Mehta et al., 2019). Based on this previous study, the effective dose at which 50% of the population are treated (ED50) of CZNPs against some multidrug resistance *E. faecium* CC17 biofilms was estimated to be 199.13 ug/mL, associated with a therapeutic index of 1.2062. However, there is still an ummet need to elucidate the physico-chemical properties of the nanomicellar CZNP that should ascertain its *in vivo* effectiveness on a broad spectrum of existing MDRs. While the effectiveness of micellar CZNPs has been previously been evidenced on a broad spectrum of some MDR pathogens (Limayem et al., 2016), some studies have confirmed the versatility of non-nanomicellar chitosan-zinc oxide formulations to cope as different nanotherapies (Al-Naamani et al., 2016, 2017; Al-Dhabaan et al., 2017; Baghaie et al., 2017; Chatterjee et al., 2017; Revathi and Thambidurai, 2018; Sathiya et al., 2018). This study herein will focus on the optimization of CZNPs nanotherapeutics in terms of physico-chemical properties for nosocomial MDR biofilms, including elucidation of biofilm protection mechanisms such as EPS, which impact human and animal host cells in addition to agricultural systems and medical devices. While this study focuses on the multifunctional capability of CZNPs as a broad spectrum antimicrobial through different levels of intricacies and habitats, the GIT is mentioned in this study herein as model for treatment due to its highest levels of complexity, with the rationale that if CZNPs can be optimized as a nanotherapeutic for the GIT, it will therefore be less difficult to repurpose it to treat infections in organ systems of a lower level of complexity (i.e., skin infections/wounds). An optimized CZNPs nanostructure, that confers high-efficacy dosing through oral administration and further overcomes physiological barriers in the GIT is required to ensure maximum potency. The highly acidic environment (low pH) along with the mucosal secretion and absorptive villi

Abbreviations: CZNPS, Chitosan combined with Zinc Oxide nanoparticles; EPS, extracellular polymeric substances; DLS, Dynamic light Scattering; PDI, Polydispersity Index; GIT, Gastrointestinal tract; ED 50, is the effective dose at which 50% of the population are treated; LD50, is the lethal dose at which 50% of the eukaryotic cells died; VRE, Vancomycin-resistant Enterococci; MDR, Multidrug resistant bacteria; TEM, Transmission Electronic Microscopy; TSB, Tryptic Soy Broth; bs, absorbance reading; FITC, Fluorescein isothiocyanate isomer; PBS, phosphate buffered saline.

constitute a major barrier for drugs to reach bacterial biofilms in the GIT. A nanomicellular delivery system of CZNPs that possesses a high-binding capacity as well as an adequate size and molecular weight to ensure a long circulating release is crucial to the success of the therapy with regard to its solubility, elasticity, and minimized opsonization (Amirmahani et al., 2017).

The overall aim, thus far, is to optimize the nanomicellar CZNP components against biofilms and their defense mechanisms to prove their capability against a broad spectrum of Gram-positive and Gram-negative MDR biofilms. *E. faecium* 1449 and *E. coli* BAA-2471 were selected in our lab as models of MDRs of the GIT due to their highly resistant and evasive virulent properties, in which out of several antibiotics tested, only tetracycline was effective (Limayem and Martin, 2014). Specific objectives herein are to evaluate CZNPs' physicochemical properties toward an improved nanostructural synthesis to elucidate EPS, a biofilm defense mechanism. The zeta potential, particle size and PDI are measured through the dynamic light scattering (DLS) technique while the morphology is observed through transmission electron microscopy (TEM). The mechanistic effects of CZNPs are measured through the biofilm inhibitory potential of CZNPs on a co-culture of MDR Gram-negative *Escherichia coli* BAA-2471 and Gram-positive *Enterococcus faecium* 1449, grown in an Alvatex 3D platform, and are further elucidated by the biofilm protectory mechanism of EPS formed in the presence of CZNPs, which is visualized using 3D confocal microscopy. This investigation, is a stepping stone to further *in vivo* therapies of infectious disease, starting from the highest level of complexity, in organ systems such as the gastrointestinal tract, to the lowest, including skin wound.

METHODS AND MATERIALS

Preparation of a Lipid-Nanomicellar CZNP Joint Formulation

The preparation of CZNPs nanomicelles as built upon from our previous studies (Limayem et al., 2015b; Mehta et al., 2019; Mohapatra and Limayem, 2019) and streamlined is as follows: to synthesize an optimized chitosan and ZnO lipid non-micellar nanoformulation (**Figures 1**, **2**), ZnO powder (∼18, 50, or 100 nm; Sigma Aldrich, St. Louis, MO) was dissolved in nano-purified water to prepare a solution of 1.42 mg/ml concentration (40 mg ZnO into 28 mL of water). This solution was sonicated for a minimum of 2–3 min to obtain a unified mixture. In the meantime, low molecular weight chitosan, derived from crab shells, (75–85% deactylated, MW: 10,000 Da; Sigma Aldrich, St. Louis, MO) was combined with 10% acetic acid solution for a concentration of 10 mg/ml, while heating and stirring the solution for about 30 min. In an attempt to prevent precipitation, the chitosan solution was heated and stirred, and after the chitosan was observed to be completely dissolved, the mixture was adjusted to pH 7 by adding 4 M sodium hydroxide dropwise. Furthermore, 25 mg of 16:0 PA 1,2-dipalmitoyl-sn-glycero-3-phosphate sodium salt (Avanti Polar Lipids, Inc., Albaster, AL) was combined with 500 μL 65:35:4:4 CH_3Cl:CH_3OH:H_2O:NH_4OH solvent solution. Nitrogen gas was used to purge this solvent. For synthesis of the micellar CZNPs, 16:0 PA lipid was incorporated via pipette into 28 mL ZnO solution, followed by 12 mL chitosan to prepare a solution with a total volume of 40 mL. The aforementioned product was sonicated for 5 min in a cold room to develop a viscous, gel-like solution.

To compare the effectiveness of ZnO-only and Chitosan-only nanoparticle solutions with CZNPs, additional ZnO-only and Chitosan-only solutions were prepared as mentioned and set aside.

Particle Size and Zeta Potential Analysis

The zeta potential, polydispersity index and particle sizes were characterized by the DLS technique using a Zetasizer (Nano-ZS, Malvern, Worcestershire, United Kingdom). All the nanoformulations were sonicated before evalution of the aforementioned properties. The samples were diluted with nano-purified water to obtain a 1:1 ratio. Three trials each were performed, with all measurements done in triplicates to achieve accurate readings.

TEM Sample Preparation and Analysis

Further characterization and visualization of CZNPs nanomicelle morphology was performed by TEM microscopy. The CZNPs samples were diluted with distilled water in a 1:250 ratio and 0.5 μm of each sample was placed on respective carbon-formvar coated grids. Each sample was allowed to settle on the grid for 2 h under an air-tight cover before the excess liquid was wafted, and the now-dry sample was loaded and visualized in the TEM.

Assessment of CZNPs Effectiveness on MDR Biofilm Models

Growth of Nosocomial MDR Biofilm Models on Alvatex Strata 3D Platform

Multi-drug resistant *E. faecium* 1449 cells were obtained from Moffitt Cancer Center (Tampa, FL) while *E. coli* ATCC BAA-2471 was acquired from American Type Culture Collection (Manassas, VA). Both the bacterial strains were cultivated separately in Tryptic Soy Broth (TSB) to a concentration of $\sim 5 \times 10^5$ CFU/mL.

The inert polystyrene Alvatex strata 3D scaffold inserts (ReproCELL Europe Ltd., Glasgow, United Kingdom) were utilized to grow MDR biofilms. The following steps were meticulously administered under sterile conditions of a biosafety cabinet. The sterile Alvatex 3D fiber platform well inserts were methodically loaded into a sterile 12-well plate. The plate was set aside after adding 3 mL of plain tryptic soy broth (TSB) media into each scaffold insert. MDR *E. faecium* 1449 colonies as well as *E. coli* BAA 2471 colonies were extracted using a previously plated culture on Tryptic soy agar (TSA), inserted into a tube of deionized water and vortexed for 10 s to obtain a 0.5 McFarland standard for turbidity. From the prepared bacterial suspensions, 1.5 μL of each was added into each well together to generate a co-culture, and the plate was incubated at 37°C for 3–5 days until bacterial growth was visible on the scaffolds. These biofilms were cautiously handled for the aforementioned time period to prevent from drying out by addition of 350

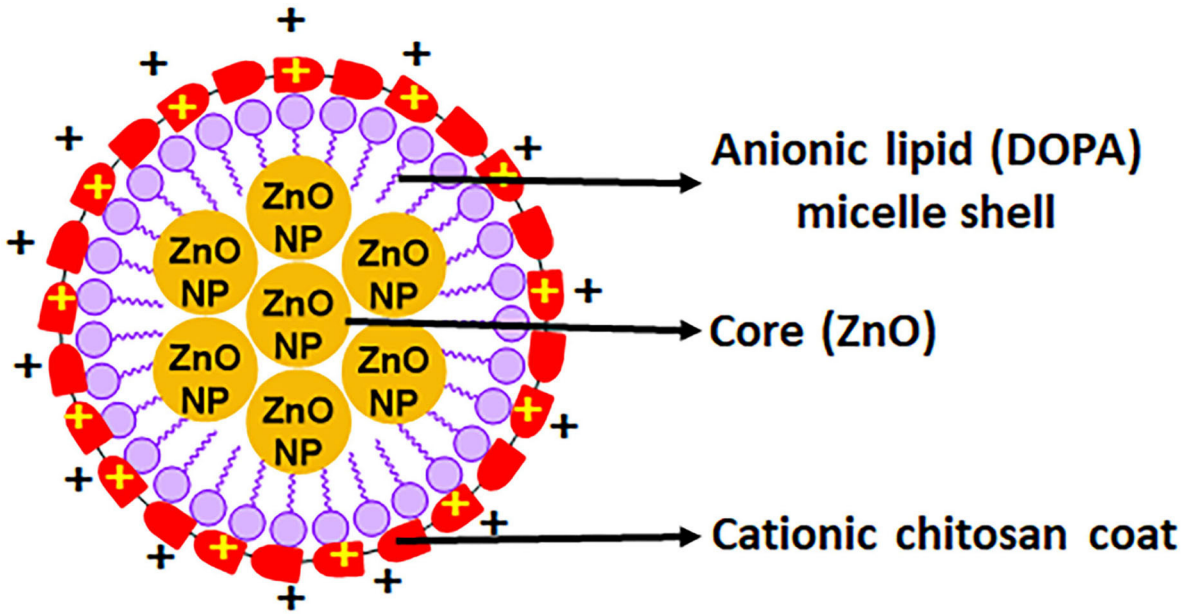

FIGURE 1 | Depiction of the charge distribution on a single nanomicelle with an anionic zinc oxide core and cationic chitosan coat.

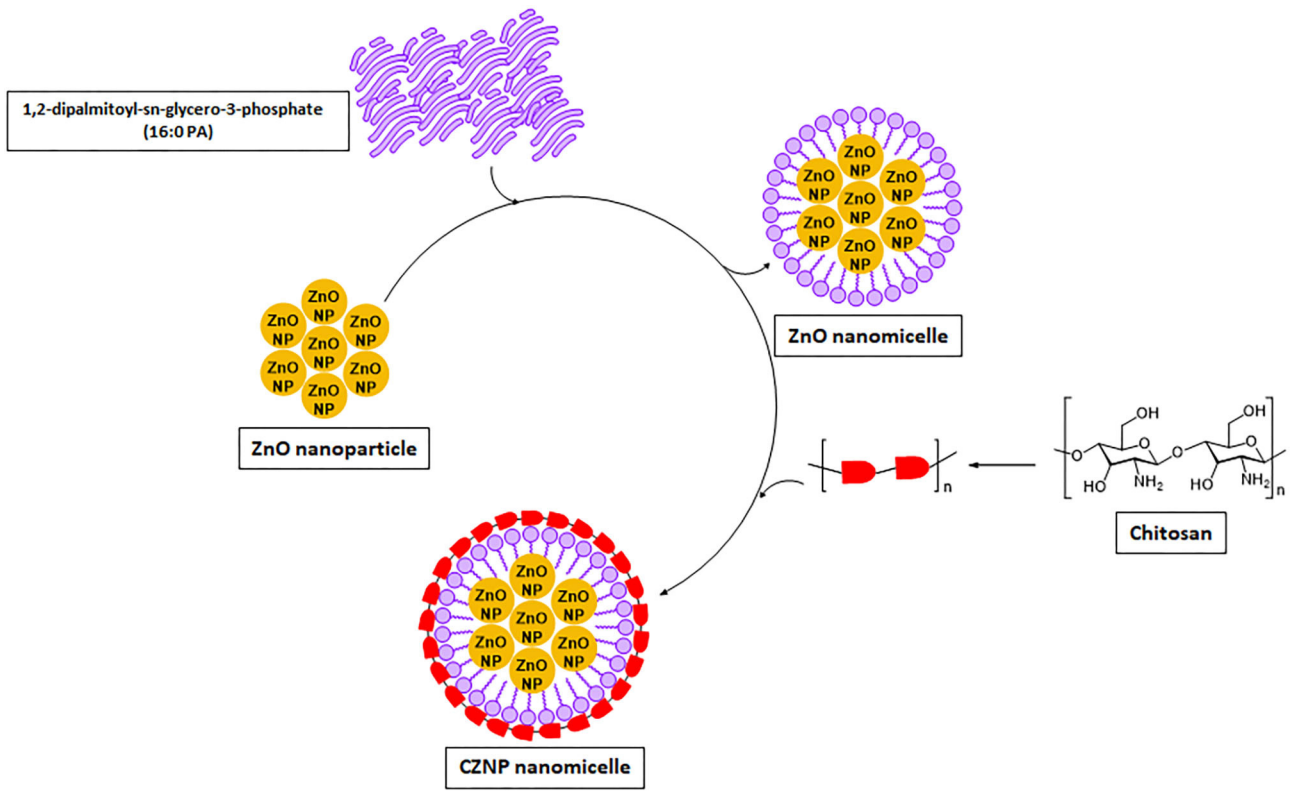

FIGURE 2 | Schematic of the stepwise preparation of the CZNP nanomicelles.

μL of TSB media. For the final step, two control wells were also plated, with the positive control consisting of bacterial suspension and the negative control using 3 mL of only TSB media instead of bacterial cell suspension. For the following assays to determine the effectiveness of the CZNPs vs. that of chitosan or zinc oxide alone on biofilm inhibition, 200 μg/mL of each testable formulation (Chitosan-only nanoparticles, ZnO-only nanoparticles and CZNPs nanomicelles) was placed into its own well and incubated further as described below.

Assay for Bacterial Structure and Extracellular Polysaccharides (EPS) Formation/Defense Mechanism

The effects of CZNPs after 72 h treatment on bacterial biofilms associated with the EPS formation were examined using a combination of fluorescein isothiocyanate isomer I (FITC) and calcofluor white M2R (CFW) dyes to stain protein and β-polysaccharide components of EPS, respectively (Ost et al., 2017; Gonzalez-Machado et al., 2018). Working solutions for stains were prepared as follows: (i) FITC–a stock solution was made by adding 2 mg of the stain in 100 μl of absolute ethanol and working solution of 46.6 μg/ml was prepared using the stock; (ii) CFW–10 mg was added to 2 ml distilled water along with 16.8 mg $NaHCO_3$ and then diluted to a working solution of 189 μg/ml. Upon dilution, both stains were added into each treated well at once, and the wells were incubated in a dark room for 25 min. After incubation, all the wells were rinsed with PBS and refilled with 250 μl of PBS.

Laser scanning confocal fluorescence microscopy imaging of the biofilms was performed through the Olympus FV1000 3D Confocal microscopy. The volume and thickness of MDRs and EPSs of the control and treated biofilms were analyzed using the 10x objective. Multiple stacks of horizontal plane images with z-step of 0.25 μm, were acquired from each well at randomly selected locations.

Quantification of Percentage Biofilm Inhibition

Toward elucidating the effectiveness of CZNPs by quantifying the biofilm reduction upon treatment, the biofilms were stained using LIVE/DEAD Viability Assay Kit (Thermofisher Scientific, Waltham, MA). A mixture of 3:3:1000 SYTO: propidium iodide: nanopurified water was created using the LIVE/DEAD Assay kit, and each target well was incubated in the dark at room temperature for 20 min with 200 μL of this mixture. Upon staining, the biofilms were dislodged from the scaffolds and were quantified using the Biotek Synergy Neo2 fluorescent microplate reader (Biotek Instruments, Winooski, Vermont). The scaffold well inserts were removed using forceps, and each of them were positioned into individual 50 mL tubes containing 7 mL of sterile PBS and 3 mL of the treatment liquid to have a total of 10 mL in each tube. The tubes were sonicated by situating them in a bath sonicator for 20 min at its maximum power. After sonication, 200 μL of the resulting cell suspension was distributed into each well of a 96 microtitre well plate. Using the Biotek Synergy Neo2 microplate reader, the wells were scrutinized under the excitation/emission frequencies of 470/510 nm for live cells and 535/617 nm wavelength for dead cells.

STATISTICAL ANALYSIS

A nested one-way ANOVA analysis of the particle size (Z-average), polydispersity index, and zeta potential was performed to determine the best particle size for CZNPs synthesis. SPSS version 24 (IBM Corporation, Armonk, New York) was used for one-way ANOVA analysis. Three independent experiments were analyzed to obtain the mean and standard deviation as well as to calculate percentage biofilm inhibition of the MDR bacteria. A Welch's ANOVA test of the biofilm inhibition experiments was done using GraphPad Prism 8.0 (GraphPad Software, San Diego, CA, USA). P-values < 0.05 were considered significant from the analyses.

RESULTS

Based on data represented by **Figure 3** and **Tables 1–3** the average CZNPs particle size for the formulation made with 18 nm ZnO was between 600 and 800 nm, which is the largest among other formulations, including those made with 50 and 100 nm ZnO (both of which had an average CZNPs particle size of ∼400 nm). The size distribution graphs may be seen in **Supplementary Figures 1–3**. The average polydisperity index for the CZNPs formulations made with 50 nm ZnO and with 100 nm ZnO is 0.393 ± 0.078 and 0.428 ± 0.045, respectively, whereas the average value for the formulation made with 18 nm ZnO is substantially higher, i.e., 0.828 ± 0.128. In terms of average zeta potential, the formulation made with 50 nm ZnO has the highest (21.7 ± 1.6 mV) compared to the ones made with 18 nm ZnO (15.4 ± 0.8 mV) and 100 nm ZnO (11.1 ± 4.4 mV). All the zeta potential values were found to be positive. The images in **Figure 4** visualize the micellar CZNPs nanoformulation synthesized using 50 nm ZnO at increasing magnifications. Lower magnifications of 4,000x depict the uniformity of the nanomicelles while the higher magnifications focus on the structural aspect of the nanomicellar formulations.

For determination of effectiveness of the optimized CZNPs against a broad spectrum of MDR bacterial biofilms, two variables were measured: EPS formation and percentage biofilm reduction. **Figure 5** represents the 3D confocal visualization (10x) of the EPS formation of the co-culture of *E. faecium* and *E. coli* upon treatment with (A) CZNPs (B) Chitosan (C) ZnO and with comparison to the positive control (D). The EPS which was stained by CFW dye and emitted blue fluorescence signals represents polysaccharides whereas those that were stained by the FITC and emitted green signals were composed of protein matter. **Figure 6** displays the result of the co-cultured biofilm treatment with CZNPs upon visualization using advanced fluorescence microscopy. The biofilms were stained with the LIVE/DEAD biofilm viability assay, which uses a combination of the SYTO 9 and propidium iodide fluorescent stains. When used in combination with each other, the SYTO 9 stains live cells, which emit a green fluorescence signal, and the propidium iodide stains dead cells, which emit a red fluorescence signal. **Table 4** represents the quantified percentage biofilm reduction values for the co-culture of *E. faecium* and *E. coli* for treatments with CZNPs, chitosan alone

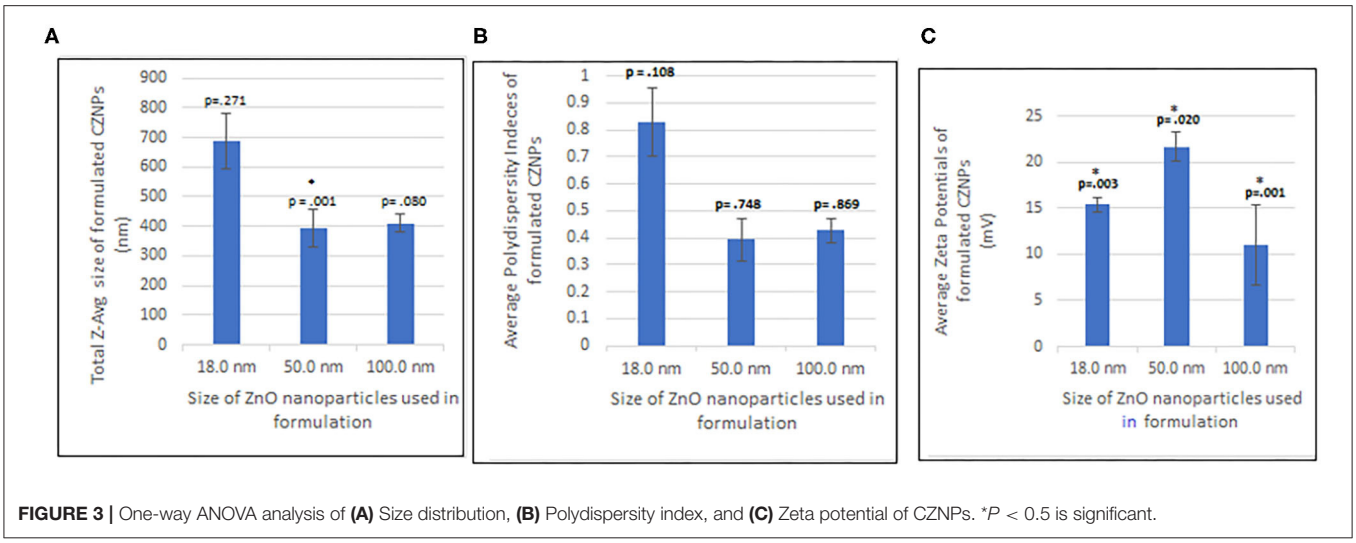

FIGURE 3 | One-way ANOVA analysis of **(A)** Size distribution, **(B)** Polydispersity index, and **(C)** Zeta potential of CZNPs. *$P < 0.5$ is significant.

TABLE 1 | Z-average size selection for CZNPs synthesis.

ZnO size (nm)	Sample #	CZNPs Z-avg size (nm)				
		Replicate 1	Replicate 2	Replicate 3	Sample average	Mean ± Standard deviation
18	1	494.1	714.3	629.6	612.7	*686.46 ± 95.32
	2	769.9	762.5	595.7	709.4	
	3	698.2	774.7	739.1	737.3	
50	4	514.7	460.0	442.7	472.5	393.41 ± 64.41
	5	392.4	359.5	355.4	369.1	
	6	335.7	337.1	343.2	338.7	
100	7	442.6	415.9	416.3	424.9	410.77 ± 30.85
	8	461.8	414.9	406.1	427.6	
	9	404.4	374.8	360.1	379.8	

*18 nm ZnO CZNPs was observed to have a higher rate of agglomeration and uneven dissolution, demonstrated by the high margin of error (Smijs and Pavel, 2011; Meibner et al., 2014).
$p < 0.001$ via one-way ANOVA.

TABLE 2 | Optimal polydispersity indices for CZNPs synthesis.

ZnO size (nm)	Sample #	Polydispesity index (PDI)				
		Replicate 1	Replicate 2	Replicate 3	Sample average	Mean ± Standard deviation
18	1	0.670	0.772	0.670	0.704	*0.828 ± 0.128
	2	0.925	0.758	0.986	0.890	
	3	0.925	0.758	0.986	0.890	
50	4	0.561	0.402	0.309	0.424	0.393 ± 0.078
	5	0.372	0.364	0.377	0.371	
	6	0.446	0.298	0.411	0.385	
100	7	0.474	0.386	0.404	0.421	0.428 ± 0.045
	8	0.512	0.411	0.400	0.441	
	9	0.471	0.395	0.400	0.422	

*18 nm ZnO CZNPs was observed to have a higher rate of agglomeration and uneven dissolution, demonstrated by the high margin of error (Smijs and Pavel, 2011; Meibner et al., 2014).
$p < 0.001$ via one-way ANOVA.

TABLE 3 | Optimal zeta potential values for CZNPs synthesis.

ZnO size (nm)	Sample #	Zeta potential (mV)				
		Replicate 1	Replicate 2	Replicate 3	Sample average	Mean ± Standard deviation
18	1	14.3	14.1	14.8	14.4	15.4 ± 0.8
	2	15.6	15.8	16.3	15.9	
	3	15.6	15.8	16.3	15.9	
50	4	21.8	22.8	22.5	22.4	21.7 ± 1.6
	5	22.4	23.5	22.5	22.8	
	6	18.4	20.2	21.2	19.9	
100	7	16.2	15.5	17.7	16.5	11.1 ± 4.4
	8	5.5	6.8	9.9	7.4	
	9	9.5	8.1	10.3	9.3	

$p < 0.001$ via one-way ANOVA.

and ZnO alone. The nanoformulations, including chitosan nanoparticles, ZnO nanoparticles, and nanomicellar CZNPs were all tested at a concentration of 200 μg/mL, based on the most effective CZNPs concentration for eradicating the MDR biofilms built from previous studies (Limayem et al., 2016; Mehta et al., 2019; Mohapatra and Limayem, 2019). The resulting fluorescence values from the Biotek Synergy Neo2 microplate reader for each treatment were compared with the positive and negative controls. Based on the results from this experiment, the percentage biofilm reduction was quantified using an optimized formula which considers the sum of the ratio of live and dead cells:

$$\%\ biofilm\ reduction = 100 * \frac{ratio\ of\ dead\ cells}{(ratio\ of\ live\ cells + ratio\ of\ dead\ cells)}$$

where the ratio of measured live cells is defined as $\frac{abs_{treatment} - abs_{negative\ control}}{abs_{positive\ control} - abs_{negative\ control}}$ determined at an excitation/emission of 470/510 nm, and the ratio of measured dead cells is defined as $\frac{abs_{treatment} - abs_{negative\ control}}{abs_{positive\ control} - abs_{negative\ control}}$ at an excitation/emission of 535/617 nm. Outliers were not considered for this analysis.

DISCUSSION

I-DLS Properties

Particle Size

Results elucidated that CZNPs formulated from 50 nm ZnO nanoparticles had the smallest average size (**Table 1**, **Figure 3A**), with a size averaging 393.41 ± 64.41 nm, followed by CZNPs made with 100 nm ZnO, with an average size of 410.77 ± 30.85 nm. Particle sizes of CZNPs were found to be disproportional with the use of 18 nm ZnO nanoparticles, denoting larger values with a higher margin of error 686.46 ± 95.32. The latter confirmed the previously documented outcomes that have reported higher rates of agglomeration and instability of nanomicelles with 18 nm ZnO nanoparticles (Smijs and Pavel, 2011; Meibner et al., 2014), thus requiring a larger size of ZnO that should generate a less aggregative nanocomponent, which is sufficiently stable for an optimal nanostructure and a successful target delivery system.

Given that nanodrugs can be either deposited or eliminated by some organs when they are administrated orally at specific sizes, the latter should be adjusted to the host cell level of complexity. For instance, a high particle size (>200 nm) of nanoformulations will be immediately removed from the bloodstream by the activated complement system and result in accumulation of the nanoformulations in the spleen and liver before reaching the targeted site (Hoshyar et al., 2016). As such, the size of CZNPs correlated to the administration routes (i.e., intravenous, oral, subcutaneous, etc.) remain of a high importance factor to drug delivery efficiency through a sustained circulation, biodistribution and release before it successfully reaches the target cell (Bahari and Hamishehkar, 2016; Lu and Gao, 2010). Therefore, if CZNPs are designed to target pathogens in the GIT, a plan on filtering the formulation through a filter size of <200 nm is required.

Polydispersity Index (PDI)

Aside from the size, the uniformity of particle size is measured as a PDI value, which ranges from 0.0 (for perfectly uniform sized samples) to 1.0 (for a highly polydisperse sample with multiple particle sizes). Thus, the measured nanocomponent size is not useful if the sample is polydisperse. Results herein, indicated that the polydispersity indices (PDIs) of the emulsions (**Table 2**, **Figure 3B**) were found to be relatively high for the 18 nm ZnO nanoparticles, ranging between 0.670 and 0.986 when compared to 50 nm and 100 ZnO nanocomponents, denoting a considerable non-uniformity in size distribution, well perceived through the high margin of error ± 95.32 and the TEM images. However, the PDI of CZNPs made from the 50 nm ZnO nanoparticles with an average PDI value of 0.393 ± 0.078, depicts greater uniformity in size distribution and dispersity than the slightly less uniform

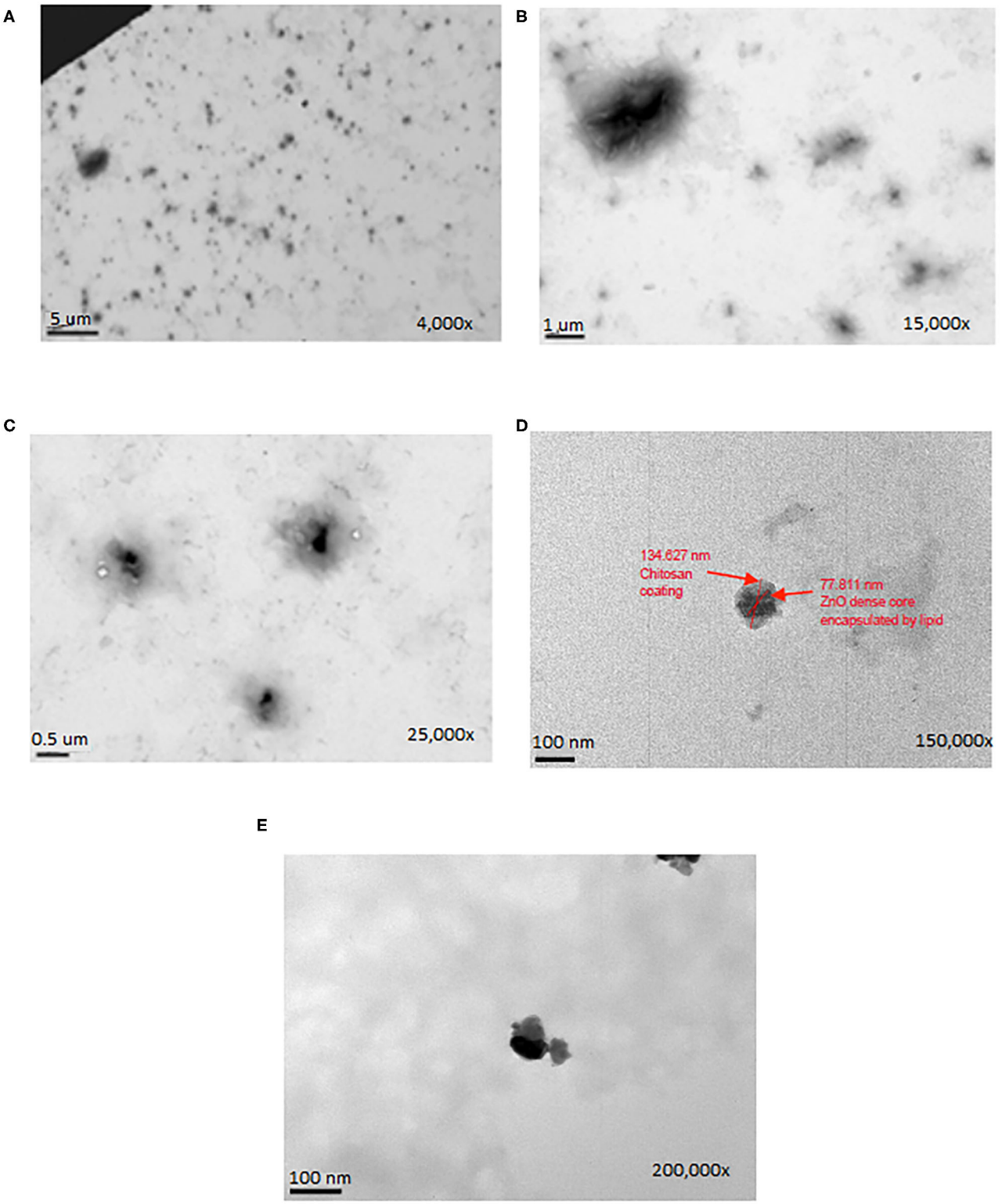

FIGURE 4 | The TEM microscopic images of CZNPs (made with 50 nm ZnO) at magnifications of **(A)** 4,000X, **(B)** 15,000X, **(C)** 25,000X, **(D)** 150,000X, and **(E)** 200,000X.

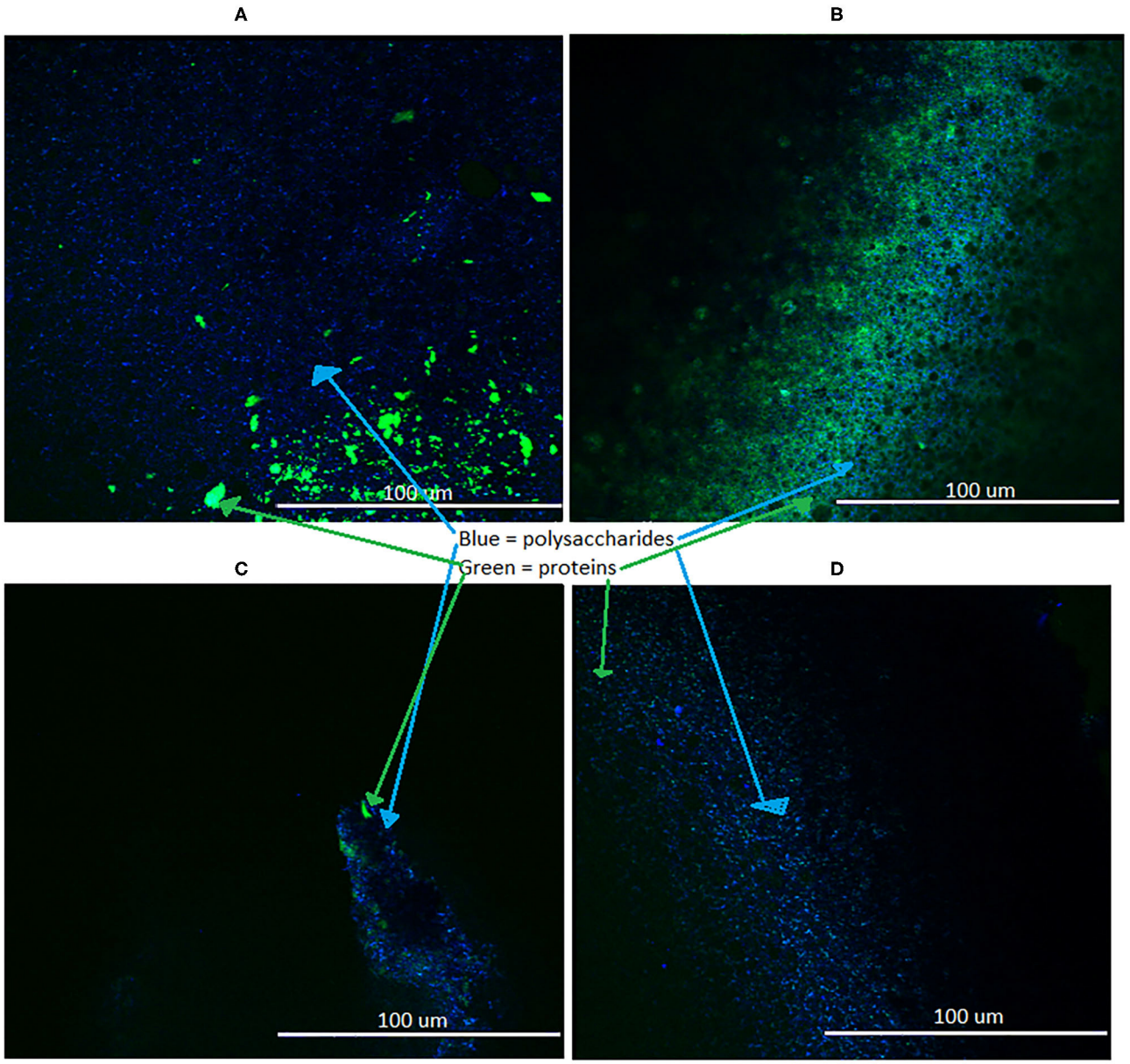

FIGURE 5 | EPS formation in biofilms treated with **(A)** CZNPs, **(B)** Chitosan, **(C)** ZnO, **(D)** no treatment control; visualized with 3D confocal microscopy at 10x.

CZNPs from 100 nm ZnO nanocomponents, having an average PDI value of 0.428 ± 0.045.

Zeta Potential

As far as the zeta potential goes (**Table 3**, **Figure 3C**), it provides a measure of the surface charge, considering the potential difference between the mobile dispersion medium and stationary layer of the medium attached to the surface of dispersed nanoformulations. It is therefore, associated with nanocomponent stability and cellular uptake in a colloidal system (Losso et al., 2005). Typically, when zeta potential values are low, the nanocomponent dispersion tends to flocculate through and forms rapid coagulation, which explains the aggregative aspect of CZNPs made of 18 nm ZnO. The CZNPs formulation made with 50 nm ZnO has the highest (21.7 ± 1.6 mV) compared to the ones made with 18 nm ZnO (15.4 ± 0.8 mV) and 100 nm ZnO (11.1 ± 4.4 mV), and all values were positive. Zeta potential values were low for both of the CZNPs nanomicelles made with the 18 and 100 nm ZnO nanoparticles (5–16 mV), which translates to an unstable formulation with higher chances of agglomeration, given that the attractive force would exceed the repulsion. While the sizes of CZNPs made from 50 to 100 nm ZnO were similar, the

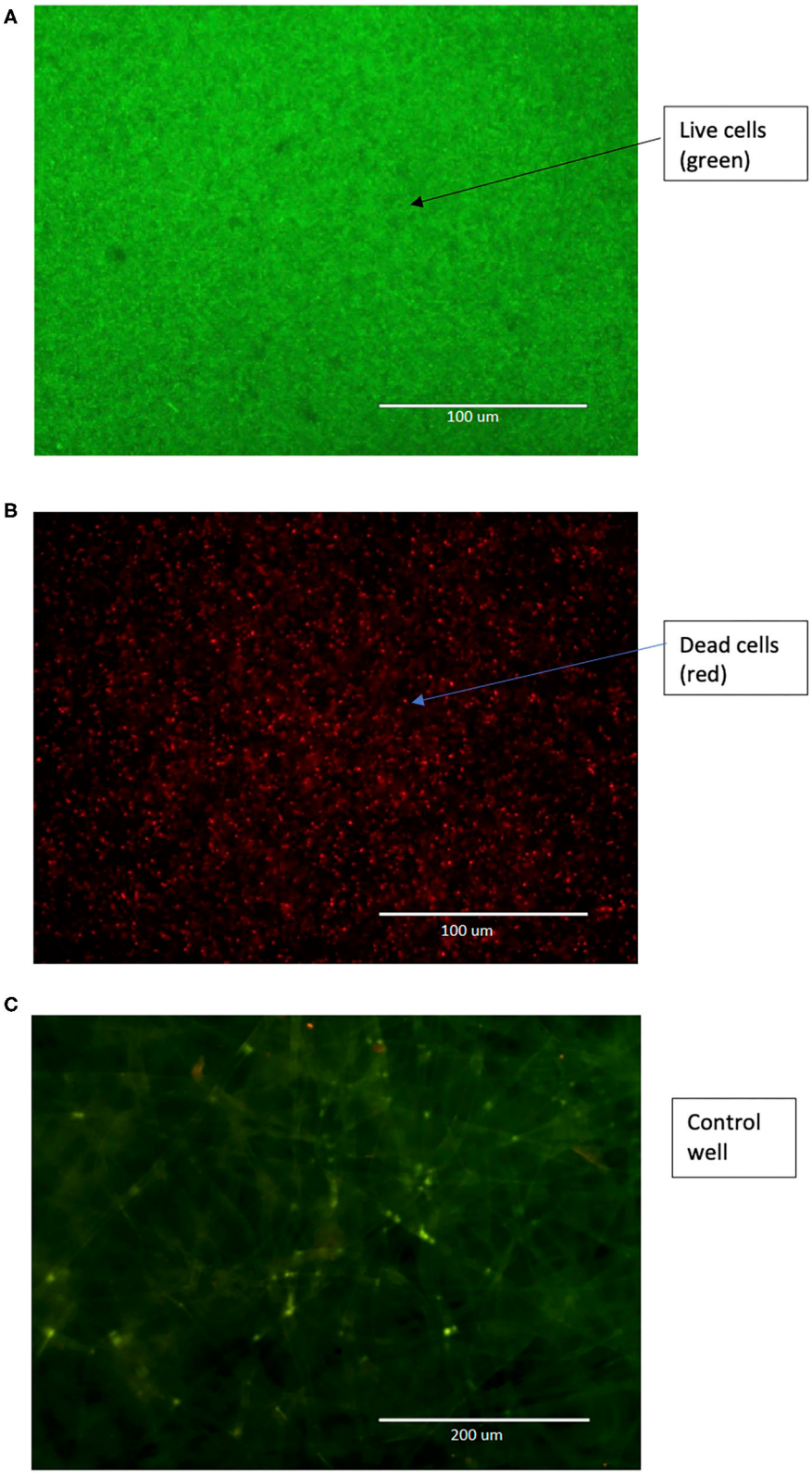

FIGURE 6 | (A) Pre-treatment and **(B)** Post-treatment (200 μg/mL CZNPs, overnight) image of co-cultured *E. coli BAA-2471* and *E. faecium 1449* biofilms at 40x magnification under GFP/RFP overlapping channel, in which live cells are stained green and dead cells are stained red. **(C)** Control image of 3D scaffold alone, with no biofilm growth, at 20x magnification under GFP/RFP overlapping channel.

TABLE 4 | Percentage inhibition of MDR *E. coli* BAA-2471 and *E. faecium* co-cultured biofilms.

	CZNPs ($n = 11$)	Chitosan only ($n = 10$)	ZnO only ($n = 9$)
Replicate 1	52.1	34.63	15.62
Replicate 2	78.63	65.42	43.2
Replicate 3	67.13	50.57	33.78
Replicate 4	53.37	39.1	34.62
Replicate 5	76.45	61.92	40.99
Replicate 6	89.32	80.28	62.08
Replicate 7	100	66.75	45.12
Replicate 8	79.78	100	100
Replicate 9	100	100	42.09
Replicate 10	100	66.04	n/a
Replicate 11	78.48	n/a	n/a
Mean ± Standard deviation	79.68 ± 17.19	66.47 ± 22.30	46.39 ± 23.52

$p < 0.0401$ via one-way ANOVA.

difference between their zeta potentials might be attributed to the pH and impurities affecting the surface charge of ZnO when the different solutions were prepared (Degen and Kosec, 2000). The CZNPs nanoformulations may possibly have a shorter shelf life because of the low zeta potential values of primarily the 18 and 100 nm ZnO.

Ultimately, based on the results of the DLS testing, ZnO particles of the size 50 nm in diameter were chosen for the optimized synthesis of uniformly sized CZNPs, resulting in the smallest sized, most stable (indicated by zeta potential) CZNPs nanomicelles with the most uniform size range, indicated by PDI. Specifically, CZNPs made with 50 nm ZnO nanoparticles resulted in sizes averaging from 338.7 to 472.5 nm, along with PDI values averaging from 0.371 to 0.424 and zeta potential values averaging from 19.9 to 22.8 mV. The most optimum of the samples tested was sample 5, which had an average size of 369.1 nm with a PDI of 0.371 and a zeta potential of 22.8 mV; sample 5 was therein chosen to have its morphology and mechanistic effects evaluated further.

II-Microscopic Visualization of CZNPs and Its Impact on Bacterial Biofilm Correlated to EPS Mechanism

TEM CZNPs Structural Observations

By observing the TEM results in **Figure 4**, it is evident that the CZNPs are well dispersed in the solution and not clustered regardless of the higher polydispersity index. Upon successive increases in magnification, the CZNPs appear to have a dark electron-dense core surrounded by an amorphous layer. The electron-dense core is representative of metallic ZnO, while the amorphous structure surrounding the ZnO core is indicative of chitosan encapsulating the ZnO due to chitosan's drug delivery capacity, as described by Zhang et al. (2004). The role of the 16:0 PA lipid in the formulation exists to stabilize the nanomicellar structure of the CZNPs as seen in **Figures 1**, **2**, enclosing the hydrophobic ZnO core with hydrophobic tails while simultaneously binding the cationic chitosan with its anionic charged head (Mohapatra and Limayem, 2019). Thus, the lipid component of the CZNPs nanomicelles is important to stabilize the overall CZNPs nanomicellar structure.

For determining the mechanistic effects of the optimized CZNPs against a broad spectrum of MDR bacterial biofilms, two variables were measured: EPS formation and biofilm inhibition. Visualization of the EPS via 3D confocal microscopy revealed the images shown in **Figure 5,** while visualization of biofilm inhibition via advanced fluorescent microscopy is shown in **Figure 6**.

Advanced Fluorescent Microscopic Biofilm Observations

Visualization of the biofilm inhibition by overnight treatment with 200 μg/mL of CZNPs was performed using advanced fluorescence microscopy in conjunction with the LIVE/DEAD biofilm viability assay (**Figure 6B**), which revealed that the majority of the biofilm was stained red, or in other words, was killed upon treatment. This is in stark contrast to the biofilm before treatment, in which all cells are stained green, indicating they are alive, and the shape of an individual bacterium is hard to discern, as there is copious biofilm growth (**Figure 6A**). These findings are supported by quantitative results as elucidated from the Biotek Synergy Neo2 (**Table 4**), which revealed that the concentration of 200 μg/mL of CZNPs was the most effective at treating the biofilm out of the formulations used, with an average co-culture biofilm reduction of approximately 79.68% in comparison to either chitosan (66.47% biofilm reduction) or ZnO (46.39% biofilm reduction) alone for the 24-h incubation period. This further confirms the effectiveness of CZNPs synergism as opposed to chitosan and ZnO alone. Moreover, based on the previous study (Mehta et al., 2019), CZNPs were determined to be more therapeutic [therapeutic index (TI) = 1.2062] than Chitosan (TI = 0.3352) or ZnO (TI = 0.0429) alone. Thus, CZNPs synergism is proved to be more effective with minimal safe threshold toxicity when compared to ZnO and chitosan alone at the same concentrations, and is a promising nanotherapeutic *in vivo* agent in suppressing MDR biofilms.

3D Confocal Microscopic EPS Observations

The EPS emitting blue fluorescence signals represents polysaccharides whereas those that emitted green signals were composed of protein matter. Overall, it was seen that the CZNPs resulted in a larger formation of both polysaccharides and proteins than the control and ZnO, and resulted in a larger formation of polysaccharides than chitosan alone. Chitosan had a larger proportion of proteins formed than CZNPs alone.

Determination of the bacterial EPS formation as a result of treatment reveals greater polysaccharide (stained blue) and protein (stained green) EPS formation in CZNPs (**Figure 5A**) and chitosan (**Figure 5B**) than that of the positive control (**Figure 5D**) and ZnO (**Figure 5C**). Specifically, CZNPs and chitosan elicited greater amounts of polysaccharide and protein EPS formation than both the positive control and the ZnO-only nanoparticles. However, chitosan elicited more protein EPS

formation than that of CZNPs, while CZNPs elicited more polysaccharide EPS formation than that of chitosan. Finally, the positive control demonstrated more polysaccharide EPS than ZnO-only nanoparticles; however, the ZnO nanoparticles elicited some protein EPS which the positive control did not. Owing to the EPS defensive mechanisms utilized by bacteria to maintain biofilm integrity and prevent penetration of the biofilm (Zhou et al., 2015), it can be inferred that CZNPs and chitosan, which resulted in the most EPS formation, formed the most stressful environment for biofilm-forming bacteria. This coupled with the biofilm inhibitory percentages, which also demonstrate CZNPs and chitosan as being the most and second most effective at inhibiting MDR biofilms, respectively, indicate that CZNPs are an effective agent at promoting stressful conditions for the biofilm-forming bacteria and subsequently suppressing them.

While the CZNPs synthesis protocol is optimized using the ZnO nanopowder of 50 nm, more experiments are recommended to further optimize the synthesis of CZNPs using 100 and 18 nm ZnO nanopowders to reduce the overall size, and to improve the polydispersity index and zeta potential values, if CZNPs are designed to target pathogens in the GIT. Perhaps the use of x-ray diffraction and neutron scattering techniques in future research studies will provide a more detailed analysis of the nanomicelle properties.

CONCLUSION

In conclusion, CZNPs are a promising alternative to suppressing MDR biofilms in future *in vivo* experiments, including testing CZNPs stability and effectiveness in acidic pH conditions to further emulate the environment of the GI tract, and subsequently in rats, as well as the *in vivo* characterization of the EPS formation by MDR bacteria in different organ systems of rats. This study suggests that the customizable CZNPs design is a promising cure of MDR infections and can be repurposed to different organ systems, ranging from the highest level of complexity (i.e., MDR-ridden GIT microbiota) to the least (i.e., drug resistant wound infections and oral cavities) Our further future studies will continue to validate CZNPs' broad-spectrum capability and effect on other microbes, such as viruses, including heat-inactivated coronavirus clumps.

DATA AVAILABILITY STATEMENT

The original contributions generated for the study are included in the article/**Supplementary Materials**, further inquiries can be directed to the corresponding author/s.

AUTHOR CONTRIBUTIONS

AL has made significant contributions to the conception and design of this work, as well as the drafting, data interpretation, and revision of this manuscript. MM has contributed significantly to the data acquisition and analysis in addition to the formatting and revision of this manuscript. SP and MN contributed toward paper collection and data acquisition for this manuscript. FC provided additional data analysis pertaining to nosocomial MDRs. All authors contributed to the article and approved the submitted version.

FUNDING

This study was funded internally by the USF Research, Innovation and Economic Development.

ACKNOWLEDGMENTS

We would like to thank the Research, Innovation and Economic Development of USF for its grant support to this research study. We also sincerely thank Moffitt Cancer Center for kindly providing the *E. faecium* 1449 cells. Furthermore, we thank the Lisa Muma Weitz Laboratory for Advanced Microscopy and Cell Imaging for providing their 3D confocal core facility access and service. Finally, we thank Dr. Manas Biswal's lab for kindly allowing us to use their Biotek Synergy Neo2 microplate reader.

SUPPLEMENTARY MATERIAL

The Supplementary Material for this article can be found online at: https://www.frontiersin.org/articles/10.3389/fnano.2020.592739/full#supplementary-material

REFERENCES

AbdElhady, M. M. (2012). Preparation and characterization of chitosan/zinc oxide nanoparticles for imparting antimicrobial and UV protection to cotton fabric. *Int. J. Carbohydr. Chem.* 2012:840591. doi: 10.1155/2012/840591

Al-Dhabaan, F. A., Shoala, T., Ali, A. A., Alaa, M., and Abd-Elsalam, K. (2017). Chemically-produced copper, zinc nanoparticles and chitosan–bimetallic nanocomposites and their antifungal activity against three phytopathogenic fungi. *Int. J. Agr. Tech.* 13, 753–769.

Al-Naamani, L., Dobretsov, S., and Dutta, J. (2016). Chitosan-zinc oxide nanoparticle composite coating for active food packaging applications. *Innov. Food Sci. Emerg. Technol.* 38, 231–237. doi: 10.1016/j.ifset.2016.10.010

Al-Naamani, L., Dobretsov, S., Dutta, J., and Burgess, J. G. (2017). Chitosan-zinc oxide nanocomposite coatings for the prevention of marine biofouling. *Chemosphere* 168, 408–417. doi: 10.1016/j.chemosphere.2016.10.033

Amirmahani, N., Mahmoodi, N. O., Galangash, M. M., and Ghavidast, A. (2017). Advances in nanomicelles for sustained drug delivery. *J. Ind. Eng. Chem.* 55, 21–34. doi: 10.1016/j.jiec.2017.06.050

Arias, C. A., and Murray, B. E. (2012). The rise of the Enterococcus: beyond vancomycin resistance. *Nat. Rev. Microbiol.* 10:266. doi: 10.1038/nrmicro2761

Baghaie, S., Khorasani, M. T., Zarrabi, A., and Moshtaghian, J. (2017). Wound healing properties of PVA/starch/chitosan hydrogel membranes with nano Zinc oxide as antibacterial wound dressing material. *J. Biomat. Sci. Polym. E* 28, 2220–2241. doi: 10.1080/09205063.2017.1390383

Bahari, L. A. S., and Hamishehkar, H. (2016). The impact of variables on particle size of solid lipid nanoparticles and nanostructured lipid carriers;

a comparative literature review. *Adv. Pharm. Bull.* 6:143. doi: 10.15171/apb.2016.021

CDC (2019). *Antibiotic Resistance Threats in the United States*. Atlanta, GA: Centers for Disease Control and Prevention, US Department of Health and Human Services.

Chatterjee, P., Ghangrekar, M. M., and Rao, S. (2017). Disinfection of secondary treated sewage using chitosan beads coated with ZnO-Ag nanoparticles to facilitate reuse of treated water. *J. Chem. Technol. Biot*. 92, 2334–2241. doi: 10.1002/jctb.5235

Degen, A., and Kosec, M. (2000). Effect of pH and impurities on the surface charge of zinc oxide in aqueous solution. *J. Eur. Ceram. Soc*. 20, 667–673. doi: 10.1016/S0955-2219(99)00203-4

Dhillon, G. S., Kaur, S., and Brar, S. K. (2014). Facile fabrication and characterization of chitosan-based zinc oxide nanoparticles and evaluation of their antimicrobial and antibiofilm activity. *Int. Nano Lett*. 4:107. doi: 10.1007/s40089-014-0107-6

Dixit, C. K., Kumar, A., and Kaushik, A. (2012). Nanosphere lithography-based platform for developing rapid and high sensitivity microarray systems. *Biochem. Biophys. Res. Commun*. 423, 473–477. doi: 10.1016/j.bbrc.2012.05.144

Fahrenfeld, N., Ma, Y., Brien, M. O., and Pruden, A. (2013). Reclaimed water as a reservoir of antibiotic resistance genes: distribution system and irrigation implications. *Front. Microbiol*. 4:130. doi: 10.3389/fmicb.2013.00130

Gonzalez-Machado, C., Capita, R., Riesco-Pelaez, F., and Alonso-Calleja, C. (2018). Visualization and quantification of the cellular and extracellular components of Salmonella Agona biofilms at different stages of development. *PLoS ONE*. 13:e0200011. doi: 10.1371/journal.pone.0200011

Gupta, U., Sharma, S., Khan, I., Gothwal, A., Sharma, A., Singh, Y., et al. (2017). Enhanced apoptotic and anticancer potential of paclitaxel loaded biodegradable nanoparticles based on chitosan. *Int. J. Biol. Macromol.* 98, 810–819. doi: 10.1016/j.ijbiomac.2017.02.030

Hoshyar, N., Gray, S., Han, H., and Bao, G. (2016). The effect of nanoparticle size on *in vivo* pharmacokinetics and cellular interaction. *Nanomedicine* 11, 673–692. doi: 10.2217/nnm.16.5

Khan, R., Kaushik, A., Solanki, P. R., Ansari, A. A., Pandey, M. K., and Malhotra, B. D. (2008). Zinc oxide nanoparticles-chitosan composite film for cholesterol biosensor. *Anal. Chim. Acta*. 616, 207–213. doi: 10.1016/j.aca.2008.04.010

Knorr, D. (1983). Dye binding properties of chitin and chitosan. *J. Food Sci.* 48, 36–37. doi: 10.1111/j.1365-2621.1983.tb14783.x

Limayem, A. (2015). Tracking *Enterococcus faecium* antibiotic resistance, dissemination and risk assessment modeling. *Agric. Food Anal. Bacteriol.* 5, 1–6.

Limayem, A., Donofrio, R. S., Zhang, C., Haller, E., and Johnson, M. G. (2015a). Studies on the drug resistance profile of *Enterococcus faecium* distributed from poultry retailers to hospitals. *J. Environ. Sci. Health Part B* 50, 827–832. doi: 10.1080/03601234.2015.1058106

Limayem, A., Gonzalez, F., Micciche, A., Haller, E., Nayak, B., and Mohapatra, S. (2016). Molecular identification and nanoremediation of microbial contaminants in algal systems using untreated wastewater. *J. Environ. Sci. Health Part B* 51, 868–872. doi: 10.1080/03601234.2016.1211912

Limayem, A., Hanning, I. B., Muthaiyan, A., Illeghems, K., Kim, J. W., Crandall, P. G., et al. (2011). Alternative antimicrobial compounds to control potential Lactobacillus contamination in bioethanol fermentations. *J. Env. Sci. Health* 46, 709–714. doi: 10.1080/03601234.2011.594411

Limayem, A., and Martin, E. M. (2014). Quantitative risk analysis for potentially resistant *E. coli* in surface waters caused by antibiotic use in agricultural systems. *J. Environ. Sci. Health B* 49, 124–133. doi: 10.1080/03601234.2014.847220

Limayem, A., Micciche, A., Haller, E., Zhang, C., and Mohapatra, S. (2015b). Nanotherapeutics for the mutating multi-drug resistant fecal bacteria. *J. Nanosci. Nanotechnol.* 1, 100106–100108.

Losso, J. N., Khachatryan, A., Ogawa, M., Godber, J. S., and Shih, F. (2005). Random centroid optimization of phosphatidylglycerol stabilized lutein-enriched oil-in-water emulsions at acidic pH. *Food Chem.* 92, 737–744. doi: 10.1016/j.foodchem.2004.12.029

Lu, G. W., and Gao, P. (2010). "Emulsions and microemulsions for topical and transdermal drug delivery," in *Handbook of Non-invasive Drug Delivery Systems*, ed V. S. Kulkarni (William Andrew Publishing), 59–94.

Mehta, M., Allen-Gipson, D., Mohapatra, S., Kindy, M., and Limayem, A. (2019). Study on the therapeutic index and synergistic effect of chitosan-zinc oxide nanomicellar composites for drug-resistant bacterial biofilm inhibition. *Int. J. Pharmaceut*. 565, 472–480. doi: 10.1016/j.ijpharm.2019.05.003

Meibner, T., Oelschlägel, K., and Potthoff, A. (2014). Implications of the stability behavior of zinc oxide nanoparticles for toxicological studies. *Int. Nano Lett.* 4:116. doi: 10.1007/s40089-014-0116-5

Mohapatra, S. S., and Limayem, A. (2019). *Compositions and Methods for Mitigating Drug Resistant Bacteria. U.S. Patent No. 10179146* (Tampa, FL: Justia Patents).

Ni, D., Bu, W., Ehlerding, E. B., Cai, W., and Shi, J. (2017). Engineering of inorganic nanoparticles as magnetic resonance imaging contrast agents. *Chem. Soc. Rev*. 46, 7438–7468. doi: 10.1039/C7CS00316A

Ost, K. S., Esher, S. K., Wager, C. M. L., Walker, L., Wagener, J., Munro, C., et al. (2017). Rim pathway-mediated alterations in the fungal cell wall influence immune recognition and inflammation. *MBio* 8, e02290–e02216. doi: 10.1128/mBio.02290-16

Ponce, A. G., Ayala-Zavala, J. F., Marcovich, N. E., Vázquez, F. J., and Ansorena, M. R. (2018). Nanotechnology trends in the food industry: recent developments, risks, and regulation. *Impact Nanosci. Food Indus*. 2018, 113–141. doi: 10.1016/B978-0-12-811441-4.00005-4

Premanathan, M., Karthikeyan, K., Jeyasubramanian, K., and Manivannan, G. (2011). Selective toxicity of ZnO nanoparticles toward Gram-positive bacteria and cancer cells by apoptosis through lipid peroxidation. *Nanomedicine* 7, 184–192. doi: 10.1016/j.nano.2010.10.001

Pruden, A., Joakim Larsson, D. G., Amézquita, A., Collignon, P., Brandt, K., Graham, D., et al. (2013). Management options for reducing the release of antibiotics and antibiotic resistance genes to the environment. *Environ. Health Persp.* 121, 878–885. doi: 10.1289/ehp.1206446

Rahman, P. M., Muraleedaran, K., and Mujeeb, V. M. A. (2015). Applications of chitosan powder with in situ synthesized nano ZnO particles as an antimicrobial agent. *Int. J. Biol. Macromol*. 77, 266–272. doi: 10.1016/j.ijbiomac.2015.03.058

Revathi, T., and Thambidurai, S. (2018). Immobilization of ZnO on Chitosan-Neem seed composite for enhanced thermal and antibacterial activity. *Adv. Powder Tech*. 29, 1445–1454. doi: 10.1016/j.apt.2018.03.007

Roy, S., Dixit, C. K., Woolley, R., O'Kennedy, R., and McDonagh, C. (2012). Synthesis and characterization of model silica–gold core–shell nanohybrid systems to demonstrate plasmonic enhancement of fluorescence. *Nanotechnology* 23:325603. doi: 10.1088/0957-4484/23/32/325603

Sabir, N., Ikram, A., Zaman, G., Satti, L., Gardezi, A., Ahmed, A., et al. (2017). Bacterial biofilm-based catheter-associated urinary tract infections: causative pathogens and antibiotic resistance. *Am. J. of Infect. Control* 45, 1101–1105. doi: 10.1016/j.ajic.2017.05.009

Sathiya, S., Okram, G., Dhivya, S., Mugesh, S., Murugan, M., and Rajan, M. A. J. A. (2018). Synergistic bactericidal effect of chitosan/zinc oxide based nanocomposites against *Staphylococcus aureus. Adv. Sci. Lett*. 24, 5537–5542. doi: 10.1166/asl.2018.12144

Sharma, A. K., Gupta, L., Sahu, H., Qayum, A., Singh, S. K., Nakhate, K. T., et al. (2018). Chitosan engineered PAMAM dendrimers as nanoconstructs for the enhanced anti-cancer potential and improved in vivo brain pharmacokinetics of temozolomide. *Pharm. Res*. 35:9. doi: 10.1007/s11095-017-2324-y

Smijs, T., and Pavel, S. (2011). Titanium dioxide and zinc oxide nanoparticles in sunscreens: focus on their safety and effectiveness. *Nanotechnol. Sci. Appl.* 4, 95–112. doi: 10.2147/NSA.S19419

Tree, J. A., Adams, M. R., and Lees, D. N. (2003). Chlorination of indicator bacteria and viruses in primary sewage effluent. *Appl. Environ. Microbiol.* 69, 2038–2043. doi: 10.1128/AEM.69.4.2038-2043.2003

Vashist, A., Shahabuddin, S., Gupta, Y. K., and Ahmad, S. (2013). Polyol induced interpenetrating networks: chitosan–methylmethacrylate based biocompatible and pH responsive hydrogels for drug delivery system. *J. Mater. Chem. B* 1, 168–178. doi: 10.1039/C2TB00021K

Yu, K., and Zhang, T. (2012). Metagenomic and metatranscriptomic analysis of microbial community structure and gene expression of activated sludge. *PLoS ONE* 7:e38183. doi: 10.1371/journal.pone.0038183

Zhang, H., Huang, X., Sun, Y., Xing, J., Yamamoto, A., and Gao, Y. (2016). Absorption-improving effects of chitosan oligomers based on their mucoadhesive properties: a comparative study on the oral and pulmonary delivery of calcitonin. *Drug Deliv*. 23, 2419–2427. doi: 10.3109/10717544.2014.1002946

Zhang, H., Oh, M., Allen, C., and Kumacheva, E. (2004). Monodisperse chitosan nanoparticles for mucosal drug delivery. *Biomacromolecules* 5, 2461–2468. doi: 10.1021/bm0496211

Zhou, G., Shi, Q. S., Huang, X. M., and Xie, X. B. (2015). The three bacterial lines of defense against antimicrobial agents. *Int. J. Mol. Sci.* 16, 21711–21733. doi: 10.3390/ijms160921711

Conflict of Interest: AL has a patent (US patent no. 10179146) licensed by Justia Patents.

The remaining authors declare that the research was conducted in the absence of any commercial or financial relationships that could be construed as a potential conflict of interest.

Copyright © 2020 Limayem, Patil, Mehta, Cheng and Nguyen. This is an open-access article distributed under the terms of the Creative Commons Attribution License (CC BY). The use, distribution or reproduction in other forums is permitted, provided the original author(s) and the copyright owner(s) are credited and that the original publication in this journal is cited, in accordance with accepted academic practice. No use, distribution or reproduction is permitted which does not comply with these terms.